



HAL
open science

X-ray phase contrast imaging model: application on tomography with a single 2D phase grating

Adrien Stolidi, Anthony Touron, Julie Escoda, Marius Costin

► To cite this version:

Adrien Stolidi, Anthony Touron, Julie Escoda, Marius Costin. X-ray phase contrast imaging model: application on tomography with a single 2D phase grating. iCT Conference 2022 - 11th Conference on industrial Computed Tomography, Feb 2022, Wels, Austria. 26580 (7 p.), 10.58286/26580 . cea-03993923

HAL Id: cea-03993923

<https://cea.hal.science/cea-03993923>

Submitted on 17 Feb 2023

HAL is a multi-disciplinary open access archive for the deposit and dissemination of scientific research documents, whether they are published or not. The documents may come from teaching and research institutions in France or abroad, or from public or private research centers.

L'archive ouverte pluridisciplinaire **HAL**, est destinée au dépôt et à la diffusion de documents scientifiques de niveau recherche, publiés ou non, émanant des établissements d'enseignement et de recherche français ou étrangers, des laboratoires publics ou privés.

X-ray phase contrast imaging model: application on tomography with a single 2D phase grating

Adrien Stolidi¹, Anthony Touron¹, Julie Escoda¹ and Marius Costin¹

¹Université Paris-Saclay, CEA, List, F-91120, Palaiseau, France, e-mail: adrien.stolidi@cea.fr

Abstract

In this paper, we propose a model dedicated to X-ray phase contrast imaging, which is well adapted to the characterization or inspection of low attenuating samples. We introduce a hybrid approach that combines a ray-tracing step with a wave propagation computation. The mathematical basis of our model is described and we present a comparison of the model to experimental results, for the case of an optical fiber sample, in the framework of a free-propagation phase technique. The extension to the 3D imaging is proposed on simulated data using a grating based technique or more precisely, a multilateral shearing interferometry. This technique uses a single 2D phase grating, which has the advantage of a simpler experimental setup and can be coupled with a standard micro-focus X-ray tube and a high-resolution detector. Our phase model was implemented on the CIVA CT simulation platform and used to generate easily different sets of projection data for any type of sample. While the method for 3D reconstruction has the same basis as the classical CT, we focus mainly on the intermediate processing steps, which are required for the phase retrieval and present the results for a phantom composed of spherical objects in different materials.

Keywords: Simulation, X-ray imaging, X-ray phase contrast, Grating-based technique, Tomography

1 Introduction

In the past decade, the transfer of X-ray phase contrast imaging methods from synchrotron-based light sources to X-ray generators revealed several challenges [1,2]. In order to assess the necessary adaptations and in order to be able to optimize certain parameters, simulation tools were an obvious choice and two approaches have been proposed in the literature: the first one based on ray tracing description and the second one based on wavefront description.

The ray tracing approach is very simple in its implementation. It consists in calculating the angle of refraction induced by the object on the path of the ray. The relative simplicity of an approach by geometrical optics, through the implementation of a ray-tracing, leads to certain limitations, highlighted by Peterzol *et al* [3]. In their study they have especially shown that the spatial coherence of the source and the detector response have to be carefully chosen with respect to the working wavelength, the object-detector distance and the magnification. The main drawback of the ray tracing approach is to not consider interference between each ray or phase variation during the propagation of the rays. To describe the interference contribution between the rays, some studies adopt a Monte Carlo ray tracing approach to model the interference effects based on the Huygens-Fresnel principle where each ray, encountering an object on its optical path, can generate secondary sources in the form of new rays which, if they exist, will be propagated to the detector [4,5]. To describe the propagation, work such as proposed by Cipiccia *et al* [6] include the propagation of rays using a time of flight calculation, with an application by Kavanagh *et al*. [7] on digital mouse phantom.

The second approach is based on the wave description. It is considered to be a more complete description than the ray tracing approach. It takes into account the phenomena of interference during the propagation of the wave. One of the first wave front model applied on laboratory source was proposed by Pogany, Gao et Wilkins [8]. Based on a Fresnel-Kirchhoff formalism, this model consider a source point and a monochromatic wave and is formulated according to the paraxial propagation. The size of the samples to inspect are always very large compared to the working wavelength λ range ($\lambda \sim 10^{-11}$ m), which makes the paraxial approximation almost correct. They have also chosen to be under the projection approximation as consequence of the paraxial approximation. This means that the effects of propagation in the object can be neglected because of the low disturbance of the sample, which is well adapted to fine or low attenuation samples, as shown by Morgan *et al* [9]. In the case where the sample is thick, the propagation of the wave within the object can no longer be neglected. Therefore, to bring a better description, especially of the effects of refraction, it is possible to discretize the space in slices perpendicular to the propagation of the wave. We can then apply a propagator to each plane and thus describe the evolution of the wavefront from slice to slice. This multi-slice approach, first described by Hare and Morrison [10], has been applied to phase imaging on a digital human phantom by Włodarczyk and Pietrak [11]. Sung *et al* [12] propose a different approach to multi-slicing, by spatially and angularly decomposing a finite X-ray source in multiple plane waves. For each plane wave at the detector, the intensity is calculated by the Rytov approximation [13] and then summed. In the Rytov approximation, we consider inside the sample and on its boundaries a progressive variation of the refractive index. This approach, not restrictive on the thickness of the object, is based on the determination of the scattering potential of object, related to the refractive index, which, according to the Rytov approximation, varies exponentially with the complex amplitude of the wave. The advantage of the wave approach, especially with the use of



the multi-slice or the object scattering potential, is a complete description of the phase effects. On the other hand, the computation time can quickly explode with, for example, a simulation time of two weeks for the simulation of a thorax [14].

Finally, hybrid approaches using a ray tracing and then a wave propagator have been investigated, especially by Peterzol *et al* [15]. In the same way, recent work of Langer *et al* [16] used Monte Carlo approach to simulate the refraction and total reflection of X-rays, coupled with an analytical wave optics approach for generating Fresnel diffraction pattern. This approach has been implemented in the medical imaging and radiotherapy simulation software GATE based on Geant4 code.

In order to address non-destructive testing applications we have recently extended the model of the radiographic and computed tomographic (RT/CT) module of CIVA [17], the multi-technique NDT simulation software developed by CEA List. Within a specific version we implemented: i) an update of the attenuation X-ray image model formation that integrates the contribution of phase contrast phenomena, through a hybrid approach that involves a ray tracing and wavefront propagation computation, ii) a phase retrieval algorithms and iii) an adapted version of CT algorithms for the 3D reconstruction of the phase distribution.

2 X-ray phase contrast imaging: direct model

2.1 Mathematical basis of the model

The developed model is built on a ray tracing and wavefront propagation. This hybrid approach makes use of the ray tracing to have a fast numerical scene description under a cone-beam configuration and of the wavefront method under the Kirchoff-Fresnel formalism to take into account the interferences and propagation. We assume a projection approximation [9, 16], which means that fine objects are assumed to have no propagation inside the object. Therefore, a transfer function $T_o(x, y)$ at the exit of the object is calculated as:

$$T_o(x, y) = \exp \left[\frac{-2\pi}{\lambda} \left\{ \int \beta(x, y, z) dz + i \int (1 - \delta(x, y, z)) dz \right\} \right]$$

where z is the propagation axis and (x, y) the perpendicular plan, λ the wavelength, and β, δ are respectively the real and imaginary part of the complex refractive index. $T_o(x, y)$ is computed using the ray tracing tool of CIVA. The established values for the individual pixels are then convoluted with a propagator $P_{od}(x, y)$. For a better efficiency, the computation is done in the reciprocal space with the Fourier Transform of the propagator $\tilde{P}_{od}(f, g)$, defined as:

$$\tilde{P}_{od}(f, g) = \exp \left[-i\pi\lambda \frac{d_{od}}{M} (f^2 + g^2) \right]$$

where M represents the magnification factor and d_{od} the propagation distance between the object and the detector. (f, g) are the spatial frequencies corresponding to (x, y) .

Gradient-based phase contrast techniques need to add a phase modulator between the source and the detector in order measure the phase variation induced by the inspected sample. Therefore, the model can take into account a second object, in addition to the numerical sample. For example, a phase grating can be added with a transfer function $T_g(x, y)$ at the exit plan of the grating and then the wavefront is propagate on the grating-sample distance with the propagator $P_{go}(x, y)$. Then, the incoming wave front at the entrance of the object $U_{in}^o(x, y)$ will be:

$$U_{in}^o(x, y) = \mathcal{F}^{-1} \{ \tilde{T}_g \times \tilde{P}_{go} \} (x, y)$$

And the wave front at the detector will be:

$$U_{det}(x, y) = \mathcal{F}^{-1} \{ \tilde{U}_{in}^o \times \tilde{T}_o \times \tilde{P}_{od} \} (x, y)$$

Based on the CIVA RT/CT existing functionality, it is also possible to use a polychromatic source, by using the implemented spectrum data base (or loading one measured spectrum) with the possibility to apply a filtration. In the same spirit, the impact of the source size s , detector response and noise on the final image can be computed. The blurring effect induced by the source size is modeled by a Gaussian function with a standard deviation σ defined as $\sigma = (s \times (G - 1))/2.35$. For the detector response, a Modulation Transfer Function (MTF) can be imported or auto generated by using an Arctan or Gaussian function parametrized by the measured spatial resolution. The detector noise could be added, depending of the type of detector used in the CIVA configuration. The photonics noise could also be added with for example a Gaussian noise (other methods are available). The scattering effect is also computed by using a Monte Carlo method. However, classical applications of X-ray phase contrast imaging are carried out with a maximum energy below 80-100 keV, hence, low contribution of the Compton scattering is usually observed. In addition, due to the projection approximation the numerical sample simulated has to be thin, which will impact the efficiency of the Monte Carlo calculation. Finally, this X-ray phase contrast imaging tool allows the use of imported Computer-Aided Design (CAD) object and handles multilateral configuration. However, these faceted objects can lead to phase image artefacts if the sampling mesh is not enough, as shown by Peterzol *et al* [3].

2.2 Comparison to experimental data

We performed several tests to validate the proposed approach. Here we present a comparison between experimental and simulated images. The object is an optical fiber made of a silicon core and ETFE cladding material (HCP M0600T). The experimental image was acquired with a laboratory setup using an X-ray microfocus generator (FeinFocus FXE 160) and a highly resolved 2D detector (Photonic Science VHR X-ray). The simulated image took into account all experimental parameters: the spectrum shape, based on the source spectral measurement following the protocol described by Plagnard [18], the spot size estimated by the NF-EN 12543-5 standard [19] and finally the detector response, measured by the CEN-EN 13068-1 standard [20]. The comparison between the experimental and simulated images is presented in Figure 1 (a,b), where a good visual agreement can be seen. In addition to this visual comparison, intensity profiles extracted from these images are presented in Figure 1 (c). The results are in good agreement and the phase curvature is well highlighted by the intensity overshoot at the object-air interface.

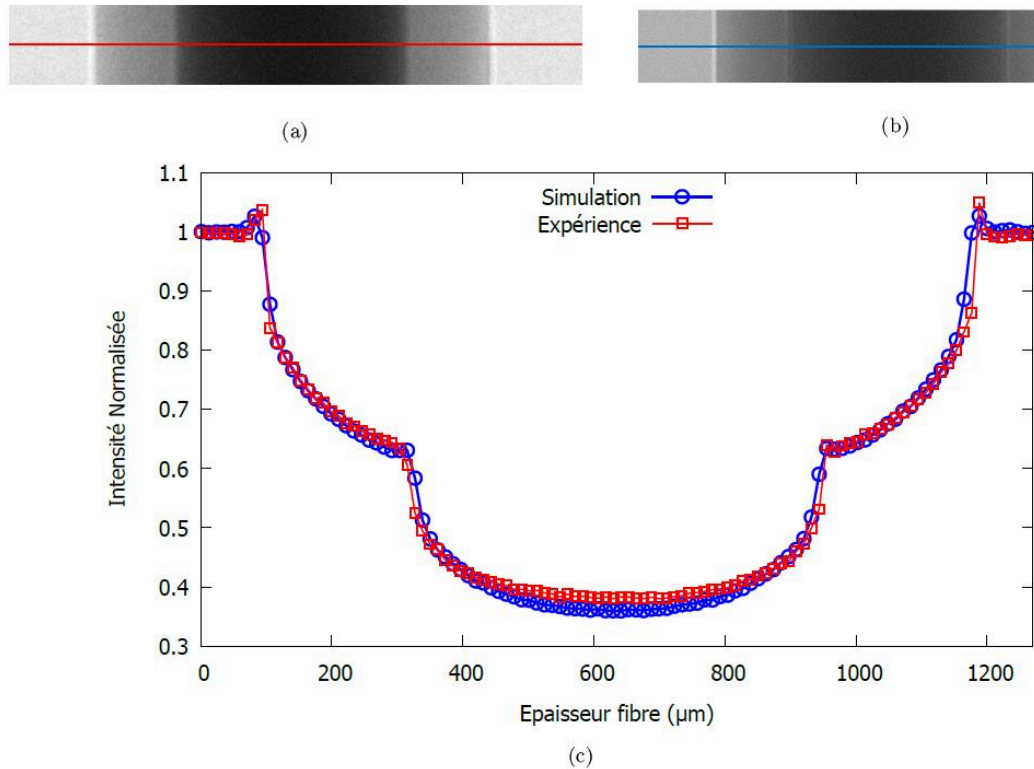


Figure 1: (a) experimental image and (b) simulated image of an optical fibre and (c) their plot profiles comparison

3 Application on radiographic images

3.1 Enhancing detectability: propagation based imaging method

The model implemented allows to take into account the phase curvature. By letting a propagation distance between the object and the detector, overshoots of intensity are visible at area where there is high variation of the refractive index value. Typically, interfaces are more highlighted by the phase curvature.

As illustration, a simulated configuration with the attenuation only model from CIVA 2021 is compared to the phase model implemented. A parallelepiped of water of 3 cm sideway, with carbon-based balls of different diameters of 300, 200, 100, 20 and 10 μm is simulated. The source of 5 μm size is monochromatic at 17 keV. The source-detector distance is fixed at 74.6 cm with an object magnification of 1.77. The image pixel size is 6 μm with an applied MTF corresponding to a spatial resolution of 5 μm . Finally, 5% of Gaussian noise is added. It can be seen that the contribution of the overshoot on the interfaces of the balls increase the detectability compared to the classical attenuation model, especially for the two last balls (see yellow arrows on Figure 2).

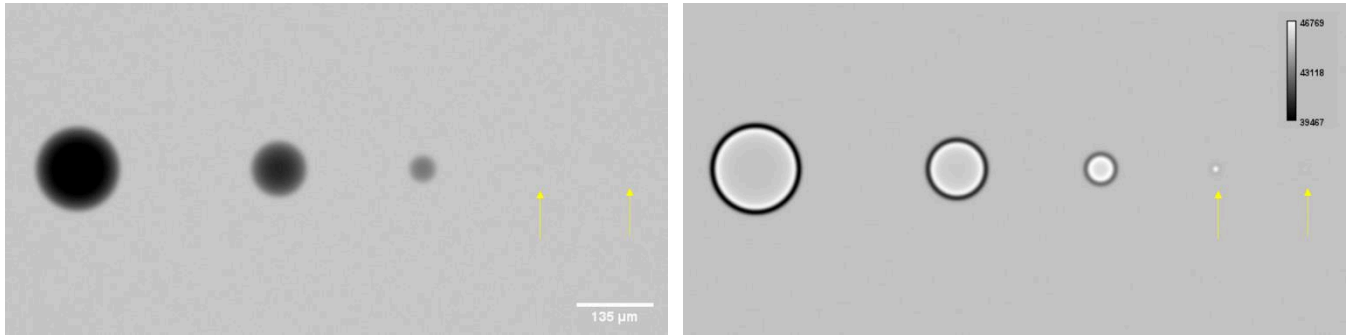


Figure 2 : simulated carbon-based ball in water of five different diameter (300, 200, 100, 20 and 10 μm). Attenuation only simulation (left) and attenuation and phase curvature (right).

3.2 Multilateral shearing interferometry: a single 2D grating technique

The Multilateral shearing interferometry (MLSI) [21] is a well-known phase sensitive technique adapted to the X-ray domain in the last decade [22], [23]. This technique allows a direct measurement of phase gradient in multiple spatial directions by using a single 2D-checkerboard phase grating. Figure 3 illustrates the MLSI procedure: first simulation of the grating is performed to get a reference image, also called interferogram. Then, the object, a carbon ball, is added, and will induce a phase shift signal, which will be sampled by the interferogram. The comparison with the reference image is performed in order to access to the phase gradient. Due to the regularity of the 2D phase grating, the phase gradient measurement could be treated in the reciprocal space by using Fast Fourier Transform (FFT). The Figure 3 (b) presents the FFT of the interferogram with the ball. All Harmonics carry a phase gradient information except the central harmonic, which carries the attenuation and phase curvature signal. Therefore, the method allow a sensitivity measurement of the phase gradient in, at least, eight spatial directions, by Fourier demodulation. Then, with two orthogonal phase gradients (Figure 3 (c)) the phase image is retrieved, Figure 3 (d), by applying the Fourier derivative theorem [10].

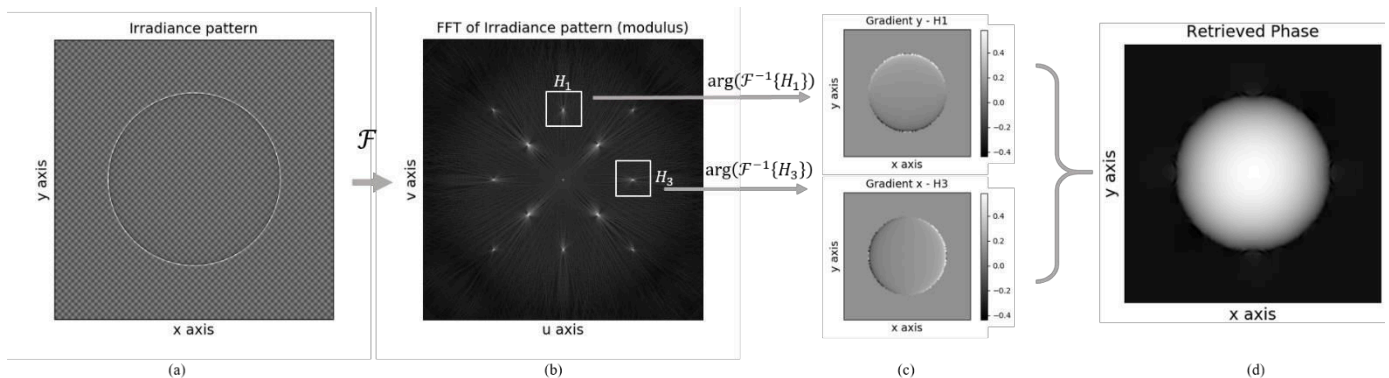


Figure 3 : simulated interferogram with a carbon-based ball (a) and it associate FFT (b). Two orthogonal phase gradients measured by Fourier demodulation (c) and based on these images the retrieved phase image (d) of the ball.

4 Phase tomography simulation and reconstruction

The phase tomography simulation is an extension of the radiographic module of the CIVA software. The simulation scene from Figure 4 presents a case with a phantom made of balls with different materials. The balls diameter is 140 μm and they are put inside a water cylinder of 900 μm diameter. The ball materials simulated, with their density ρ , are Chlorine ($\rho = 0.003 \text{ g/cm}^3$), Carbon ($\rho = 2.25 \text{ g/cm}^3$), Aluminum ($\rho = 2.173 \text{ g/cm}^3$), Sodium ($\rho = 0.9 \text{ g/cm}^3$), Titanium ($\rho = 4.54 \text{ g/cm}^3$) and Air ($\rho = 0.001 \text{ g/cm}^3$). A phase grating is added to the scene in order to be able to measure phase gradient signals, based on the MLSI method. It is a 2D checkerboard grating of gold with a thickness of 4 μm and orthogonal periodicity of 12 μm . A set of 360 projections of angular step of 1° is simulated. For this configuration, a polychromatic source is simulated with the maximal energy of 40 keV and a sampling spectrum of 1 keV. The final pixel size is 6 x 6 μm^2 . Two configurations with noise at 5% and without noise are considered for the classical attenuation model implemented in CIVA 2021 software and the proposed phase model. The computation time for the phase model is less optimized with a simulation running of 13 hours and 40 minutes compared to the attenuation model in CIVA 2021 with a computation time of 2 hours and 30 minutes, performed with a processor Intel(R) Core(TM) i7-8850H CPU 2.60 GHz and a RAM memory of 32 Go.

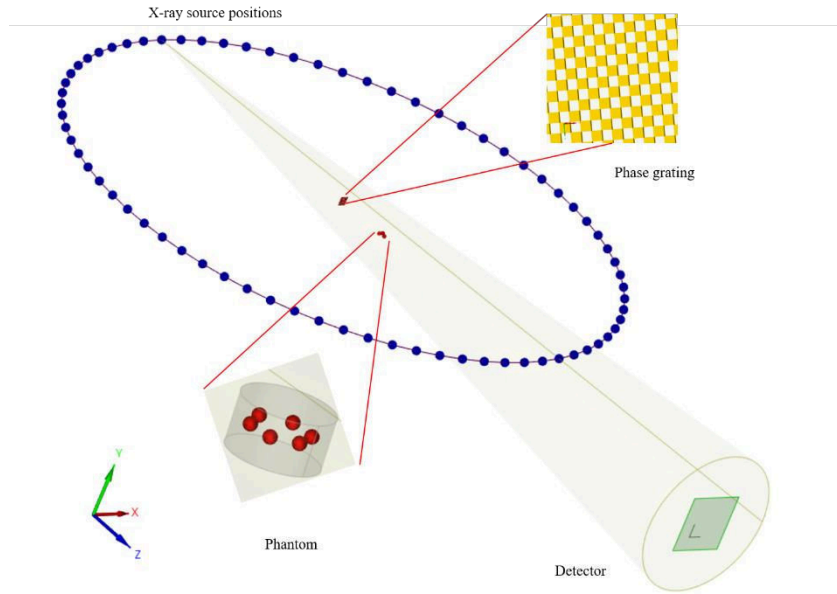


Figure 4: Example of phase CT simulation in a MLSI setup using CIVA software

The figure 5 (a) presents the simulation results for one projection. In addition to the interferogram produced by the grating and the water cylinder, the balls with high densities and high atomic number Z are highlighted by the attenuation information (left and center of the water cylinder). Low attenuation balls are less visible (see for example on the right of the water cylinder). However, for this last case, the phase gradient on Figure 5 (b) gives a better contrast. It can be noted on the gradient image that artefacts are present on the edges of the balls especially on the diagonal axis. This is due to an under sampling effect. Indeed, the phase curvature present at the edges is a very fast intensity variation with low spatial spreading. In this case, the fringes periodicity is not sufficient to sample it. Therefore, phase aliasing artefact appears. It is even more important for the ball presenting an important density and/or for the high- Z ball material because the signal to noise ratio (SNR) of the fringes is greatly reduced by their attenuation, which will induce diminution of the phase gradient measurement. Because the phase image is extracted from the phase gradients images, these artefacts are reported on the phase image (Figure 5 (c)).



Figure 5: simulation result for one projection (a). The corresponding phase gradient (b) and phase image (c)

Figure 6 presents the results of both considered simulation configurations with, on the top, the attenuation simulation results including one of the 360 projections and a reconstructed slice without and with 5% of noise (respectively Figure 6 (a,b,c)) and on the bottom the same data for the phase simulation (Figure 6 (d,e,f)). The material of each ball is reported on the central column. Figure 6 (b,c) present the reconstruction of the attenuation coefficient, based on projections simulated with a classical version of CIVA 2021 (Figure 6 (a)), without phase modeling. They can be directly compared with the results presented on Figure 6 (e,f) obtained from the projections simulated with the phase model implemented. The applied 3D phase reconstruction algorithm is derived from the classical FDK algorithm. Due to the MLSI phase retrieval algorithm, no additional pretreatments of the input projections are applied, which means that no log conversion and ramp filtration are needed for the 3D phase reconstruction. Classical FDK is used for the 3D attenuation reconstruction.

The 3D phase reconstruction of the phantom brings complementary contrast to the classical attenuation simulation as expected. Compared to the attenuation reconstruction, the edge of the water cylinder of the phase slice exhibits a sort of cup artefact (Figure 6 (e,f)). Its nature is due to the under sampling of the over intensity induced by the refractive index variation between the outside and inside of the water cylinder as seen on the projections (Figure 6 (d)). The phase aliasing, mentioned before, is less present on the edges of the balls due to a smoothing effect of the reconstruction algorithm but are distributed inside the water cylinder. Low density materials such as air and Chlorine are more contrasted on the phase reconstruction compared to the attenuation slice. The high attenuation of the Aluminum and Titanium allows a proper contrast on the attenuation reconstruction but brings, in this configuration, metal artefacts. It is interesting to note that these two metallic elements are also well reconstructed in the phase volume without creating such artefact. (see Figure 6 (e)). Finally, the more interesting case is the complementary contrast between the two configurations for the Carbon and Sodium balls. Indeed, Carbon has the same attenuation as the water but induces a notable phase shift. On the other hand, the Sodium ball of 140 μm thickness has a phase value comparable to the water cylinder of 900 μm thickness for the polychromatic illumination simulated, while it has a different attenuation value. The slices reconstructed with noisy projections (Figure 6 (c,f)) show a limited impact of the noise on the contrast given by the phase and the attenuation signal but streak artefacts are increased on both configurations. Compared to the attenuation configuration, the phase reconstruction displays blurred edges of the balls. This is due to the poor sampling of the interference fringes bringing a less spatially resolved phase projection.

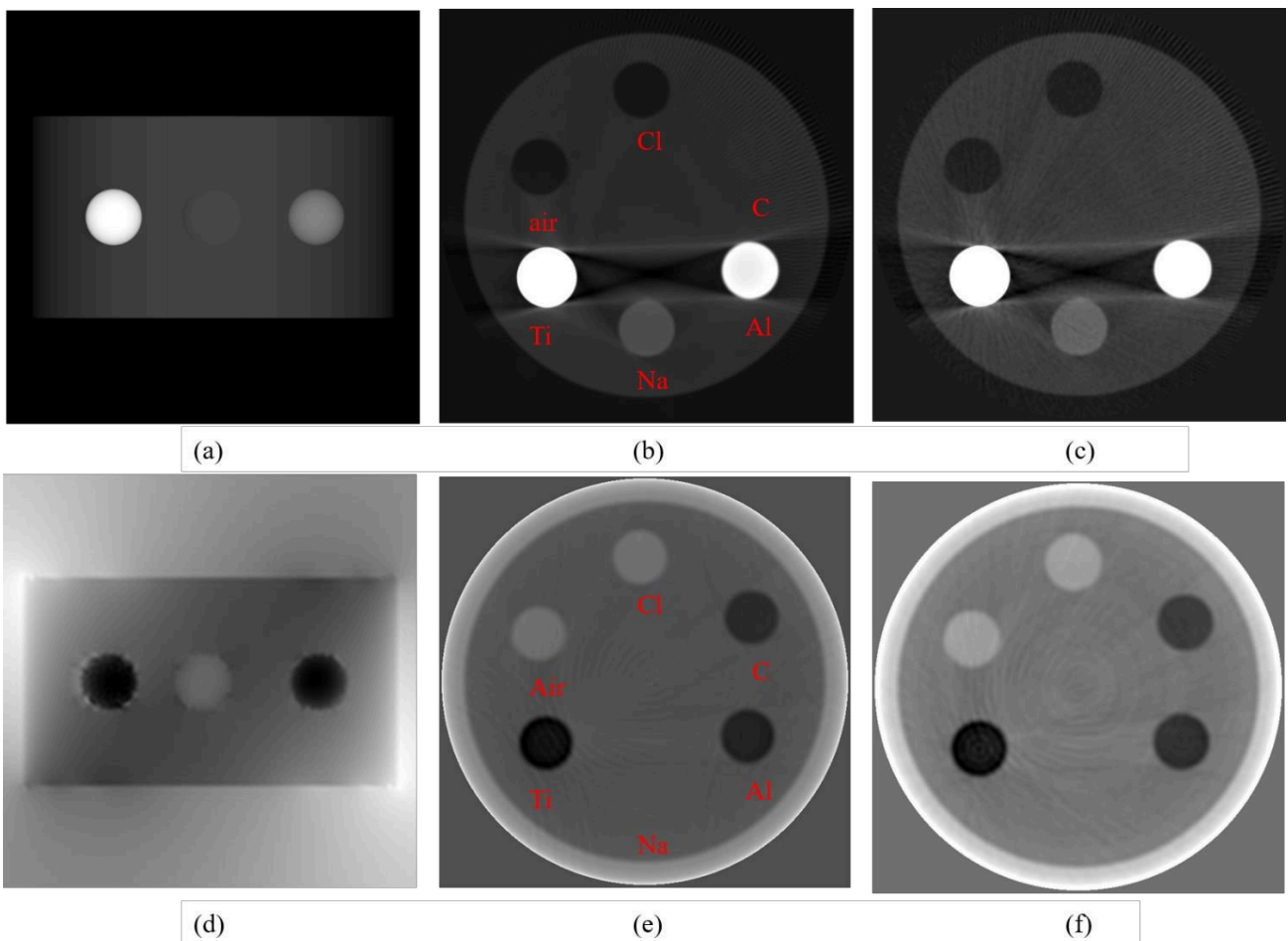


Figure 6: Two numerical configurations based on attenuation (top row) and phase (bottom row) simulations with an example of projection (left column) and the corresponding slices reconstruction without (central column) and with 5% noise (right column).

5 Conclusions and perspectives

This work presents a first implementation of an X-ray phase contrast model on CIVA software. In addition to the already implemented attenuation model of CIVA RT/CT, a calculation of the phase variation induced by an object is done under the projected approximation, using the ray tracing approach, and then propagated onto the detector using a wavefront model. Experimental parameters can be simulated such as polychromatic spectrum of the source, influence of the X-ray spot size, grating positioning, use of multilateral object, detector response and noise. First simulated phase CT acquisition have been presented on

regular trajectory with reconstructed volume of a simple phantom based on an adaptation of the FDK reconstruction algorithm. A comparison with classical attenuation CT simulation and reconstruction has been also presented.

For the near future, more details phase CT simulations of a carbon-based phantom will be conducted with contrast and spatial resolution evaluation and comparison to classical attenuation CT simulations. A particular attention will be paid to the interpretation of the grey levels induced by the phase slices, in comparison of the attenuation slices.

Finally, future works will focus on the extension of the direct model by taking into account the propagation inside the object. Adaptation of iterative reconstruction algorithm will be also targeted. Indeed, in the context of high-resolution tomography using phase contrast technique such as MLSI, acquisition time can be significant. It is therefore important to adopt a strategy to reduce it by, for example, reducing the number of projections.

Acknowledgements

The authors want to acknowledge the precious insight provided by Dr. Jérôme Primot from ONERA, and also Véronique Colombié and Thibaud Fortuna from CEA List for their implementation of the single phase grating model in CIVA.

References

- [1] M. Endrizzi, "X-ray phase-contrast imaging," *Nuclear Instruments and Methods in Physics Research, Section A: Accelerators, Spectrometers, Detectors and Associated Equipment*, vol. 878. Elsevier B.V., pp. 88–98, Jan. 11, 2018, doi: 10.1016/j.nima.2017.07.036.
- [2] A. Momose *et al.*, "X-ray phase imaging: from synchrotron to hospital," *Philos. Trans. R. Soc. A Math. Eng. Sci.*, 2014.
- [3] A. Peterzol, A. Olivo, L. Rigon, S. Pani, and D. Dreossi, "The effects of the imaging system on the validity limits of the ray-optical approach to phase contrast imaging," *Med. Phys.*, 2005.
- [4] A. Prodi *et al.*, "A Monte Carlo approach for simulating the propagation of partially coherent x-ray beams," 2011.
- [5] E. Bergbäck Knudsen *et al.*, "McXtrace: a Monte Carlo software package for simulating X-ray optics, beamlines and experiments," *J. Appl. Crystallogr.*, 2013.
- [6] S. Cipiccia, F. A. Vittoria, M. Weikum, A. Olivo, and D. A. Jaroszynski, "Inclusion of coherence in Monte Carlo models for simulation of x-ray phase contrast imaging," *Opt. Express*, 2014.
- [7] A. Kavanagh, A. Olivo, R. Speller, and B. Vojnovic, "Feasibility testing of a pre-clinical coded aperture phase contrast imaging configuration using a simple fast Monte Carlo simulator," *Biomed. Opt. Express*, 2014, doi: 10.1364/BOE.5.000093.
- [8] A. Pogany, D. Gao, and S. W. Wilkins, "Contrast and resolution in imaging with a microfocus x-ray source," *Rev. Sci. Instrum.*, 1997.
- [9] K. S. Morgan, K. K. W. Siu, and D. M. Paganin, "The projection approximation and edge contrast for x-ray propagation-based phase contrast imaging of a cylindrical edge," *Opt. Express*, 2010.
- [10] A. R. Hare and G. R. Morrison, "Near-field soft X-ray diffraction modelled by the multislice method," *J. Mod. Opt.*, 1994.
- [11] B. Włodarczyk and J. Pietrzak, "Analytical reconstructions of intensity modulated x-ray phase-contrast imaging of human scale phantoms," *Biomed. Opt. Express*, 2015.
- [12] Y. Sung, C. J. R. Sheppard, G. Barbastathis, M. Ando, and R. Gupta, "Full-wave approach for x-ray phase imaging," *Opt. Express*, 2013.
- [13] Y. Sung and G. Barbastathis, "Rytov approximation for x-ray phase imaging," *Opt. Express*, 2013.
- [14] Y. Sung, W. P. Segars, A. Pan, M. Ando, C. J. R. Sheppard, and R. Gupta, "Realistic wave-optics simulation of X-ray phase-contrast imaging at a human scale," *Sci. Rep.*, 2015.
- [15] A. Peterzol, J. Berthier, P. Duvauchelle, C. Ferrero, and D. Babot, "X-ray phase contrast image simulation," *Nucl. Instruments Methods Phys. Res. Sect. B Beam Interact. with Mater. Atoms*, 2007.
- [16] J. M. Létang, M. Langer, S. Rit, and Z. Cen, "Towards Monte Carlo simulation of X-ray phase contrast using GATE," *Opt. Express*, Vol. 28, Issue 10, pp. 14522–14535, vol. 28, no. 10, pp. 14522–14535, May 2020, doi: 10.1364/OE.391471.
- [17] M. Costin *et al.*, "CIVA CT, an advanced simulation platform for NDT." Accessed: Oct. 21, 2020. [Online]. Available: www.ndt.net/?id=18774.
- [18] J. Plagnard, "Mesure de spectres en énergie de l'émission de tubes à rayons X au LNE-LNHB / LMD Measurement of the LNE-LNHB / LMD X-ray tube spectra by X-ray spectrometry," pp. 37–47.
- [19] NF - EN 12543-5, "Non-destructive testing. Characteristics of focal spots in industrial X-ray systems for use in non-destructive testing. Part 5 : measurement of the effective focal spot size of mini and micro focus X-ray tubes," 1999.
- [20] CEN - EN 13068-1, "Non-destructive testing - radioscopic testing - Part 1: Quantitative measurement of imaging properties," 1999.
- [21] J. Primot, "Three-wave lateral shearing interferometry," *Appl. Opt.*, 1993.
- [22] J. Rizzi, P. Mercère, M. Idir, P. Da Silva, G. Vincent, and J. Primot, "X-ray phase contrast imaging and noise evaluation using a single phase grating interferometer," *Opt. Express*, 2013.
- [23] A. Stolidi, G. Giakoumakis, J. Primot, A. Jarnac, and D. Tisseur, "Confidence Map tool for gradient-based X-ray phase contrast imaging," *Opt. Express*, Sep. 2021, doi: 10.1364/OE.438876.
- [24] R. Bracewell, "The fourier transform and its applications," *McGraw-Hill Electr. Electron. Eng. Ser.*, vol. 5, 1965.